Effect of Precursor Solution Aging on the Crystallinity and Photovoltaic Performance of Perovskite Solar Cells

*Hsinhan Tsai, Wanyi Nie, Yen-Hao Lin, Jean Christophe Blancon, Sergei Tretiak, Jacky Even, Gautam Gupta, Pulickel M. Ajayan, and Aditya D. Mohite**

Perovskite materials due to their exceptional photophysical properties are beginning to dominate the field of thin-film optoelectronic devices. However, one of the primary challenges is the processing-dependent variability in the properties, thus making it imperative to understand the origin of such variations. Here, it is discovered that the precursor solution aging time before it is cast into a thin film, is a subtle but a very important factor that dramatically affects the overall thin-film formation and crystallinity and therein factors such as grain growth, phase purity, surface uniformity, trap state density, and overall solar cell performance. It is shown that progressive aging of the precursor promotes efficient formation of larger seeds after the fast nucleation of a large density of small seeds. The hot-casting method then leads to the growth of large grains in uniform thin-films with excellent crystallinity validated using scanning microscopy images and X-ray diffraction patterns. The high-quality films cast from aged solution is ideal for thin-film photovoltaic device fabrication with reduced shunt current and good charge transport. This observation is a significant step toward achieving highly crystalline thin-films with reliability in device performance and establishes the subtle but dramatic effect of solution aging before fabricating perovskite thin-films.

1. Introduction

The rapidly improving certified photovoltaic (PV) cell power conversion efficiency (PCE), which now exceeds 22%[1,2] has made hybrid perovskite-based materials the rising star among solution processed thin-film PV technologies, which placed them into the center stage of the thin-film PV research community.[3–16] The near exponential rise in photovoltaic performance is attributed to perovskites remarkable properties such as strong optical absorption[17,18] giving rise to highly mobile[19,20] free charge carriers that can migrate up to few microns.[7,8,21,22] Moreover, perovskite family is extremely tunable system that can incorporate a broad variety of organic cations[4,14,23–32] or anions[33–36] into perovskite structure that provides chemical synthetic means to control the optical absorption[4,25–27,29] and improve photo- and environmental stability by passivation of the interfaces.[4,29,37,38] While tremendous progress has been made in the past few years, one of the key challenges in the field of hybrid perovskites today[9,15,39–45] is the dependence of the optoelectronic properties of hybrid perovskites thin films predominantly on the processing conditions.[12,13,40,46–48] Subtle changes in preparation of the precursors or processing conditions, can lead to a substantial variation in the physical properties of the thin films and, as a result, in the observed experimental data.[13,49–53] The latter in turn has resulted in nonconsistent physical interpretations across the research community. The variability often finds its origins in nonuniform film coverage,[47,54–56] defect densities,[57,58] migration of ions or vacancies,[59–62] which directly compromise the overall crystallinity and thus also the device reliability and stability.[3,9,12,13,63] There have been several reports illustrating a wide range of processing techniques for improving the crystallinity of the perovskite thin films.[3,11,13,47,64–68] However, very limited studies were performed on understanding the correlation between the nucleation process within the precursor solution and how it influences the formation of the final perovskite thin film.

H. Tsai, Prof. P. M. Ajayan
Materials Science and Nanoengineering
Rice University
Houston, TX 77005, USA

H. Tsai, Dr. W. Nie, Dr. G. Gupta, Dr. A. D. Mohite
Materials Physics and Application
Los Alamos National Laboratory
Los Alamos, NM 87545, USA
E-mail: amohite@lanl.gov

Dr. Y.-H. Lin
Department of Chemical and Biomolecular Engineering
Rice University
Houston, TX 77005, USA

Dr. J. C. Blancon
Physical Chemistry and Applied Spectroscopy
Los Alamos National Laboratory
Los Alamos, NM 87545, USA

Dr. S. Tretiak
Theoretical Chemistry and Molecular Physics
Los Alamos National Laboratory
Los Alamos, NM 87545, USA

Prof. J. Even
Fonctions Optiques pour les Technologies de l'Information
FOTON UMR 6082
CNRS, INSA de Rennes
35708 Rennes, France

DOI: 10.1002/aenm.201602159

Recent works have demonstrated that PbI_2-MAI (MA = methylammonium) intermediate phase formation by certain choice of solvents and additives can serve as a nucleation seed and also facilitates crystal growth process.[11,69] While these studies suggest that nucleation within the precursor is important, outstanding questions remain on the precursor aging time, its impact on thin-film crystalline quality, uniformity, and their correlation with solar cell performance and trap state density.

Here, we report for the first time, that the aging time of the precursor solution is subtle but a very important parameter that controls the efficacy of nucleation, thin film growth, uniformity (or film coverage), and trap state density, all of which directly determine the crystalline quality and in turn the overall performance of any optoelectronic device. We show that there is a progressive formation of very large seeds (or crystallites) during the aging process of the precursor solution that are important for achieving high-quality thin-film growth with good conversion to the perovskite phase. We observe that with increasing solution aging time above 24 h, the film quality improves significantly as evidenced by larger grain features.[3,70–72] We correlate the improved film quality to the efficient formation of large seeds characterized using atomic force microscopy (AFM) and scanning electron microscopy (SEM) on thin films. We also evaluate the crystallinity of these perovskite thin films using X-ray diffraction (XRD) and observe a direct correlation between the precursor aging time and the degree of conversion and crystallinity of the desired perovskite phase. As expected, we observe that the solar cell performance is also correlated with the solution aging time and for the optimal aging time of 48 h, we measure an average PCE exceeding ≈15% average efficiency in a planar device architecture. The reproducible and high PCE is attributed to the improved thin film quality—crystallinity and coverage—and thus reduced shunt resistant and lower defect density in the devices prepared from an aged precursor solution. We anticipate that this discovery is a significant step toward achieving highly crystalline thin films with a high degree of reliability in device performance and establishes the subtle but dramatic effect of solution aging before making perovskite thin films.

2. Results and Discussion

Figure 1 illustrates the impact of precursor aging time composed with lead iodide (PbI_2) and methylammonium hydrochloride (MACl) in dimethylformamide (DMF) (from 1 to 48 h maintained at 70 °C in an argon-filled glove box) on the grain-like features. The feature sizes are measured using optical microscopy by averaging the apparent grains on perovskite thin films synthesized using our recently reported hot-casting method[3,4,40,46,49,71] on an Indium tin oxide (ITO)/Poly(3,4-ethylenedioxythiophene)-poly(styrenesulfonate) (PEDOT:PSS) substrate. The substrate temperature for hot casting was maintained at 180 °C for all the substrates before spin coating the precursor solution aged for different time periods. The typical optical microscopy images for film cast from the various aged solutions are illustrated in Figure 1a–d. The results indicate that there is a progressive increase in the

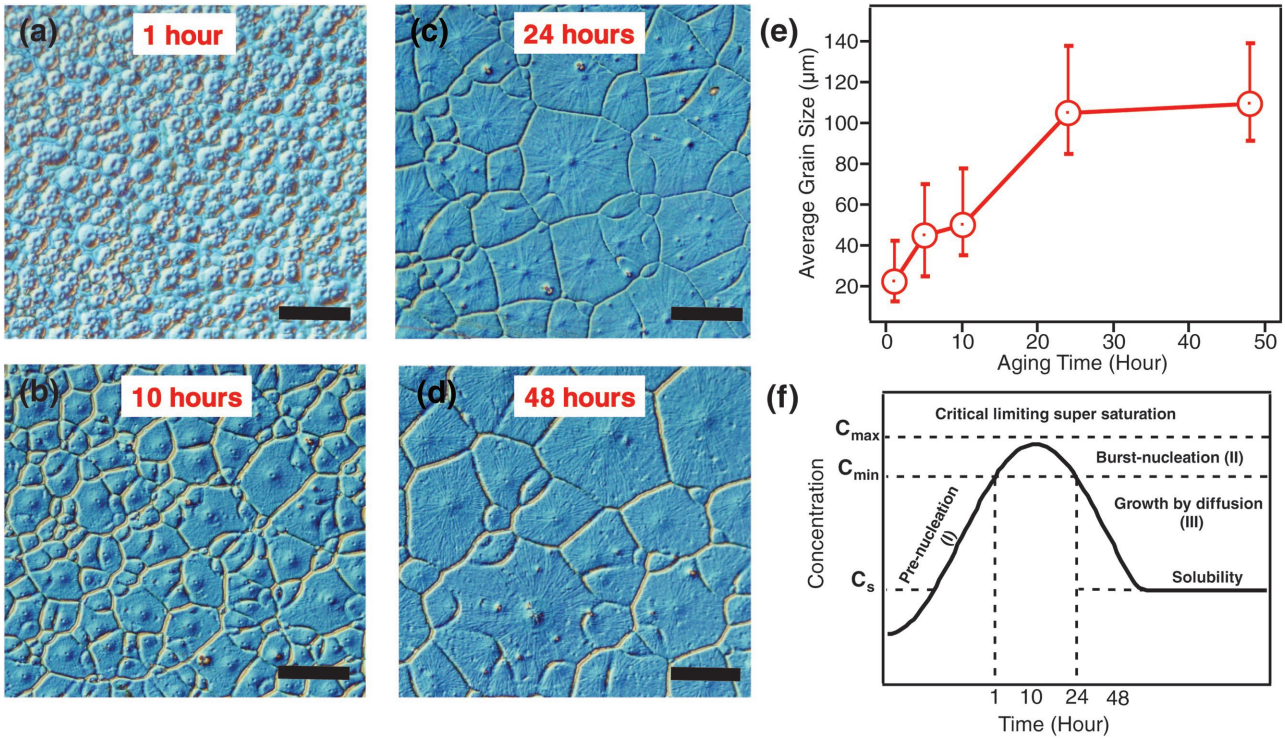

Figure 1. Optical microscope images of perovskite thin films produced by hot casting. The precursors are aged at different time points a) 1 h, b) 10 h, c) 24 h, and d) 48 h. The grain size varies from ≈20 to ≈110 μm (Scale bar: 50 μm). e) Average grain-size with error bar determined for 1–48 h aging time. f) LaMer diagram for crystallite formation stages in solution.

grain size with the precursor solution aging time. We further plot the average grain size as a function of precursor solution aging time as shown in Figure 1e. The average grain size is calculated by taking the statistical distribution of the linecut over the optical image and sampling over 50 grains and over five different optical microscopy images. Within the first 10 h, the average grain sizes vary between 20–50 μm. When the aging time reaches 24 h, the average grain size dramatically increases to 105 μm. Then, it slowly increases and saturates to 110 μm at 48 h. The detailed measurement of grain size distribution is provided in Figure S1 (Supporting Information). To understand the obtained results, we suggest that the grain growth process is strongly correlated with the nucleation of seeds within the precursor solution. These observations on the precursor aging effect can be well described using a LaMer diagram,[73–76] (see Figure 1f) which describes the process of the effect of precursor aging as three distinct regimes: (I) Prenucleation: rapid increase in the concentration of PbI_2 and MACl free intermediates. (II) Burst-nucleation: fast nucleation of Pb-MA-I/Cl complex in the precursor solution. (III) Growth by diffusion: decrease in concentration of PbI_2-MAI/Cl complex by forming larger crystallites. The precursor was made using PbI_2 and MACl, and the characterizations indeed reveal that a mixture of $MAPbI_3$ and $MAPbCl_3$ is formed. The beneficial role of chloride-based precursors for efficient nucleation has been well demonstrated previously in solar cell applications.[50,77–79] At different time points, we take the precursor and characterize with UV–vis absorption and XRD (Figures S2 and S3, Supporting Information), then further make thin films using the hot-casting method. The resulting properties of precursor solution and the hot cast film are a direct reflection of the evolution of the PbI_4^{2+} complex phase in precursor solution.[80] We first examine the thin film made from 1 h aged solution. The optical image shows that the majority features consist of small grains in the thin film, which suggests that after 1 h the prenucleation, stage I within the precursor solution has ended. Precursor aging period of 1–10 h solutions represents a burst-nucleation stage II dominated by a large density of small seeds, therefore, the obtained thin film rapidly evolves into a large number of small grains as illustrated in Figure 1a,b. After the short period of burst-nucleation, the thin film aged for 10 h shows the formation of larger grains (Figure 1b) in comparison to the 1 h aged precursor. This implies that the precursor solution has transitioned from the burst nucleation stage II to the growth stage III. Moreover, the size distribution of 1 and 10 h in Figure S1 (Supporting Information) clearly suggests a low dispersity of the initial nuclei distribution, which is typical indication of a LaMer growth process.[74] Finally, the latter occurs in the precursor solution leading to the formation of larger seeds (or crystallites) in the precursor solution. The growth stage is reminiscent of Ostwald ripening[73,81] where small crystallites redissolve and deposit onto intermediate size crystallites to form large seeds, which is consistent with previous reports of MABr treatment in $MAPbI_3$.[82] Once we take the growth stage III solution and cast thin film with hot casting method, the large grain features are observed (see Figure 1c,d). Herein, we emphasize that the high quality bulk-like thin film resulting from those large size grain feature facilitates the fabrication of planar device with negligible shunt current[3,49] and allows for observation of the intrinsic optoelectronic properties through the film without parasitic effects from the boundaries.[46]

To validate our hypothesis that the presence of nucleating seeds and their size in the progressively aged precursor solution is directly correlated with observed grain size and crystallinity, we drop cast the precursor solutions into thin films (at same concentration without heating) on a silicon wafer substrate to directly estimate the size of the seeds within the precursor by examining the roughness using AFM (see **Figure 2**a–c). Figure 2d–f are the linecuts derived from the AFM images in Figure 2a–c, which further illustrates the increase in the size of the seeds from 1 to 48 h of precursor aging. From the AFM images, the thin film cast from 1 h aged precursor has a very high density of seeds with a mean size of ≈177 nm, consistent with burst-nucleation stage II described above. For the 24 h aged precursor solution, average size of the seeds is measured to be ≈274 nm, which further increases to ≈559 nm for the 48 h aged solution, indicating the solution reaches growth stage III. Complimentary to our inference of the crystallize size using AFM images, we performed dynamic light scattering experiments on the precursor solution aged at various times. The results are illustrated in Figure S4 in the Supporting Information, which shows that as the solution aging time increases, the crystallite size (in diameter) increases from 190 nm for 1 h solution to above 500 nm for 48 h solution. These results clearly suggest that with increasing the precursor aging time, the size of the seeds in the precursor also increases. Subsequently, this results in the formation of large grains when converted to the perovskite phase using the hot-casting technique.

Motivated by the correlation between the size of the seeds with aging of the precursor solution and the resulting grain sizes in thin films, we performed SEM and grazing incidence X-ray diffraction (GIXRD) studies to evaluate the microstructure and crystalline quality of the resulting thin films produced from precursors aged at different times from 1 to 48 h as illustrated in **Figure 3**. First, we examine the SEM cross section of hot-cast thin films with 1 and 48 h aged precursor solution as shown in Figure 3a,b, respectively. The thin film made with 48 h aged precursor has much more uniform, pinhole free, and compact layer compared to the film made using a 1 h aged solution. Furthermore, the cross-section SEM images across the thin films show that the films cast from 48 h aged solution are bulk like and extend uniformly parallel to the substrate. Figure 3c shows the diffraction patterns for each time stamp with red circle and green triangle representing methylammonium lead iodide ($MAPbI_3$) and methylammonium lead chloride ($MAPbCl_3$), respectively. It is well known that using this specific stoichiometric combination (PbI_2+MACl), the chlorine perovskite ($MAPbCl_3$) phase is relatively easily formed due to the large difference in the ionic radii of Cl^- and I^- anions[49,53,77] and crystal formation speed.[50,77,83] The $MAPbCl_3$ phase is a wide bandgap semiconductor (bandgap = 3.11 eV)[53,84] and is considered an undesired phase as it exists heterogeneously, resulting in nonconductive regions in the perovskite thin films. Our results show that as the aging time increases, the XRD peak ratio of $MAPbI_3$/$MAPbCl_3$ increases dramatically as

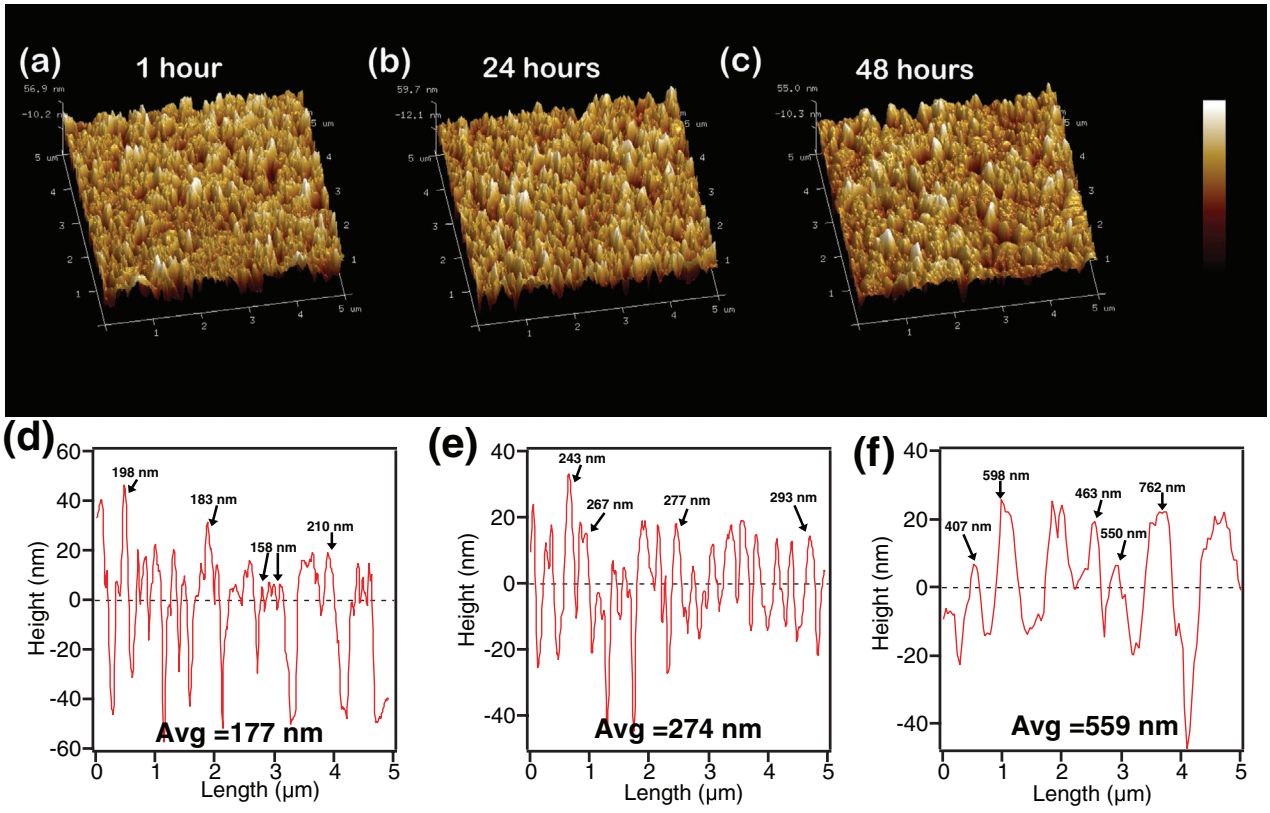

Figure 2. Topography images of AFM for perovskite thin film spin coated from precursor aged for a) 1 h, b) 24 h, and c) 48 h. Panels d–f) are the linecut analysis from panels a–c). The analysis demonstrates the crystal size increase with the aging time. These observations are consistent with literature-proposed nucleation process.

shown in Figure 3d. For 1 h precursor, the XRD peak ratio for $MAPbI_3/MAPbCl_3$ is 1.55 in the thin film (40% $MAPbCl_3$ phase). However, the XRD peak ratio increases to 2.73 (26.8% $MAPbCl_3$ phase) when the solution is aged for 24 h. We also examine solvent impact on the precursor solution with dimethyl sulfoxide (DMSO). The results suggest that the $MAPbI_3/MAPbCl_3$ peak ratio is higher than DFM as solvent and changed over time (see Figure S5 in the Supporting Information), which are suggested that DMSO is a stronger coordination solvent and has similar effect as DFM. Along with the peak ratios, Figure 3d also shows the full width half-maximum (FWHM) of the $MAPbI_3$ peak at 14.28° (110). With increasing aging time, the thin-film crystallinity is dramatically improved as can be evaluated from the FWHM, which progressively decreases, until it becomes almost constant for more than 24 h of aging. Both GIXRD and FWHM results indicate that 24–48 h precursor aging is ideal for achieving good crystalline quality. This result also indicates that a desired $MAPbI_3$ phase is forming more effectively from the aged solution. Surprisingly, we find that between 24 and 48 h of precursor aging, the $MAPbI_3$ peak starts to decrease. This is probably due to the replacement of I^- anions in $MAPbI_3$ with Cl^- anions over such long aging times, because Pb—I bond strength is much weaker than Pb—Cl one,[85] thus there is a strong propensity for the replacement of I^- anions with Cl^- anions.[86] Moreover, from the initial work by Lifschitz and Slyozov[87] on Ostwald ripening, suggests that the vacancies are expected to play a specific role during the growth process. Near the edges, the nucleus cavities tend to dissolve and the vacancies diffuse to the surface. This could also favor the I–Cl exchange at the surface. Based on these results, we show that a careful tuning of the precursor solution aging time can be used to limit the formation of the undesired $MAPbCl_3$ phase and to improve the efficacy of the formation of the desired $MAPbI_3$ phase, which is critical for achieving homogeneity in perovskite thin films.

To correlate our structural and thin film properties with device performance, we fabricated planar solar cells using an inverted architecture and the results are illustrated in **Figure 4**a. Here, the perovskite thin films prepared using the hot-casting method with precursors aged at varying time intervals as described earlier and PEDOT:PSS and [6,6]-phenyl C_{61} butyric acid methyl ester (PCBM) were used as the hole and electron transport layers, respectively. The *J–V* characteristic curves measured under air mass 1.5 Global 1 Sun for different aging times of perovskite solutions are shown in Figure 4b. It can be clearly observed that, as the precursor aging time elongated progressively from 1 to 48 h, the average power conversion efficiency also increased from ≈2.5% to ≈15%. Moreover, we also found that once the precursor solution is aged beyond 24 h, it results in highly crystalline films that do not exhibit any appreciable hysteresis (see Figure 4c). The summary of the solar cell figures of merit as a function of different aging times is illustrated in Figure 4d–g. The average open-circuit voltage (V_{OC}) in Figure 4d

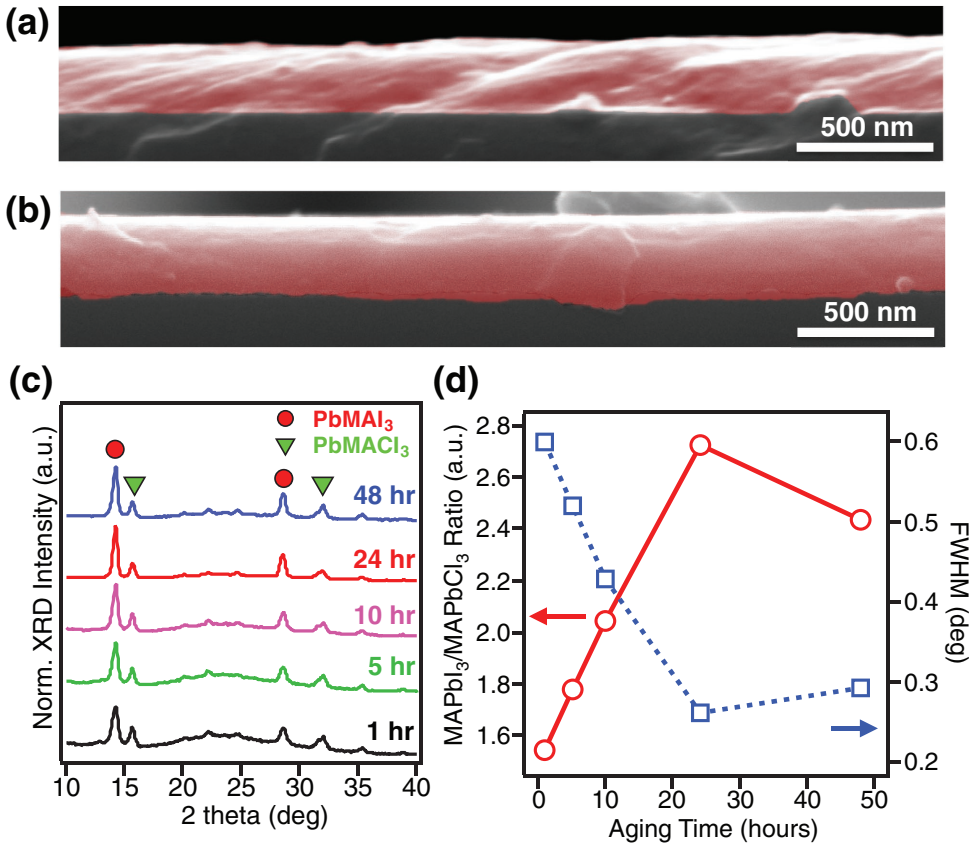

Figure 3. Thin films characterization. Cross-section SEM images of perovskite thin film from a) 1 h and b) 48 h aged precursor solution. c) Grazing incidence X-ray diffraction (GIXRD) of different age time from 1 h to 48 h, showing the ratio of the desired $PbMAI_3$ and unwanted $MAPbCl_3$ phases. d) Peak ratio of $MAPbI_3/MAPbCl_3$ as function of aging time and FWHM of $MAPbI_3$ peak ($2\theta = 14.28°$) clearly suggesting that the 24–48 h aged thin film has the optimal peak ratio and crystallinity.

does not change appreciably, which is consistent with our previous study that beyond 20 µm grain size, the V_{OC} remains constant.[3] The increase in PCE is mainly due to the dramatic increase in current density (J_{SC}) and the fill factor (FF), which are illustrated in Figure 4e,f, respectively. The average PCE for the various aging time periods follows the trend set by the current density and fill factor. As a result, the device cast from 48 h solution has the best performance with average PCE of 15.22 ± 0.45%, V_{OC} of 0.94 ± 0.021 V, J_{SC} of 20.92 ± 0.94 mA cm^{-2}, and fill factor of 77.58 ± 0.32%. As can be seen from the J–V curves, the improvement on J_{SC} with the progressive solution aging time of the casting precursor can be attributed to increased $MAPbI_3$ phase (Figure 3d) in the thin films leading to a better absorption near the band edge (see Figure S6 in the Supporting Information). Moreover, the improvement in the fill factor is directly related to the improved crystallinity and uniform coverage of the thin film on the substrates. According to the J–V curve measured under 1 Sun, the current is higher from the maximum power point toward the smaller field (open circuit) condition for the devices fabricated from 24 h aged precursor in comparison with device fabricated from 1 h, indicative of the suppressed recombination of charge carriers and a good charge transport of carriers. The slope near short circuit point is also reduced for the devices fabricated from 24 h aged in comparison to the device fabricated from 1 h implying a reduced shunt current through pinholes or regions with nonuniform thickness on the thin films.

Finally, we performed the impedance spectroscopy measurement on the 1 h device as compare to the 48 h device. The capacitance–frequency spectrum is shown in **Figure 5**a and the phase analysis for those two devices are shown in Figure 5b. Also, the calculated trap density of states is presented in Figure 5c. From the results, the capacitance response toward the low frequency region shows a steep increase for the nonaged device while a much flat curve is observed for the aged device. In the phase analysis, the nonaged device shows a decrease in phase from 100 to 0.1 Hz range while the aged device does not show such an increase until 10 Hz. This is related to the low frequency dielectric loss due to the shunt in the device.[88] When large numbers of grain boundaries exist in the film, the film coverage tends to be nonuniform across the device as evidenced by the cross-section SEM images shown in Figure 3a. Those shunts or current leakages are reflected in the light J–V curves by the steep slope near J_{SC}. And those shunts (pinhole or vacancies) can also act as a recombination center that reduces the open-circuit voltage. We therefore take the frequency range of 100–10^5 Hz for trap states analysis and the result is shown in Figure 5c. From the trap density of state spectrum, the trap state density are comparable in both of the cases, however, the aged device tend to shift the trap state peak

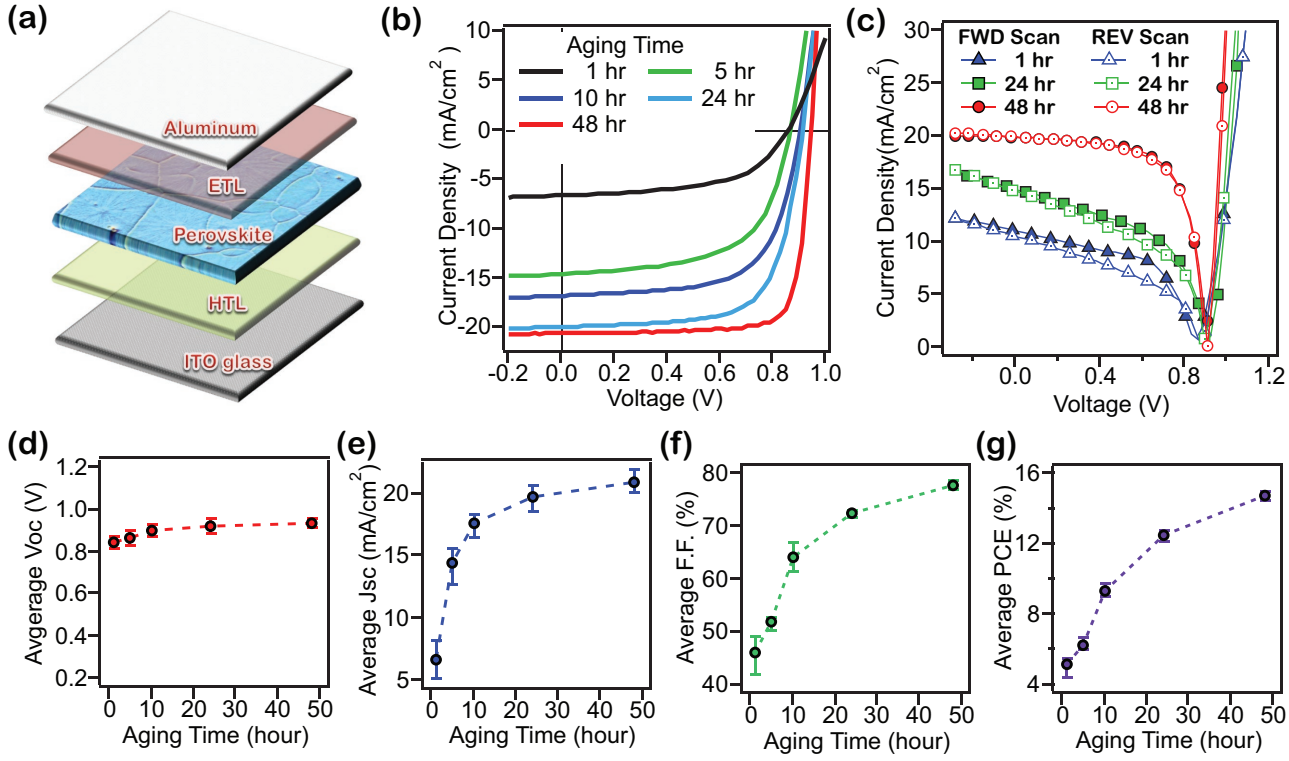

Figure 4. Photovoltaic performance as a function of precursor solution aging times: a) Planar architecture of perovskite solar cell used in this article. b) *J–V* characteristic curves and c) hysteresis test of perovskite devices with different aging times. d) Averaged open-circuit voltage (V_{OC}), e) current density (J_{sc}), f) fill factor (FF), and g) power conversion efficiency (PCE) in devices performance.

toward lower frequency (2×10^4 Hz) than the nonaged device (peaks at 8×10^3 Hz), which is correlated to a more shallow trap energy. By reducing the grain boundaries in the device, it could suppress the charge recombination and thus improve the charge collection.

3. Conclusion

We report a strong correlation between solution aging time and thin-film crystallinity in hybrid $MAPbI_3$ perovskite material system. Structural characterization reveals that the ratio of $MAPbI_3/MAPBCl_3$ is enhanced upon aging. Furthermore AFM studies on the as cast solution elucidate the key role of nucleation within the precursor solution with progressive aging. The results suggest that once the precursor solutions aged for more than 24 h, the crystallinity and grain-like features of perovskite are dramatically improved. We also show that structure and composition of the perovskite films have a direct impact on the photovoltaic device performance and characteristics. Thus, in summary, we have demonstrated that precursor aging represents an essential discovery for not only researchers working on perovskite materials but in general when precursors are converted to thin films by nucleation and crystal growth during the

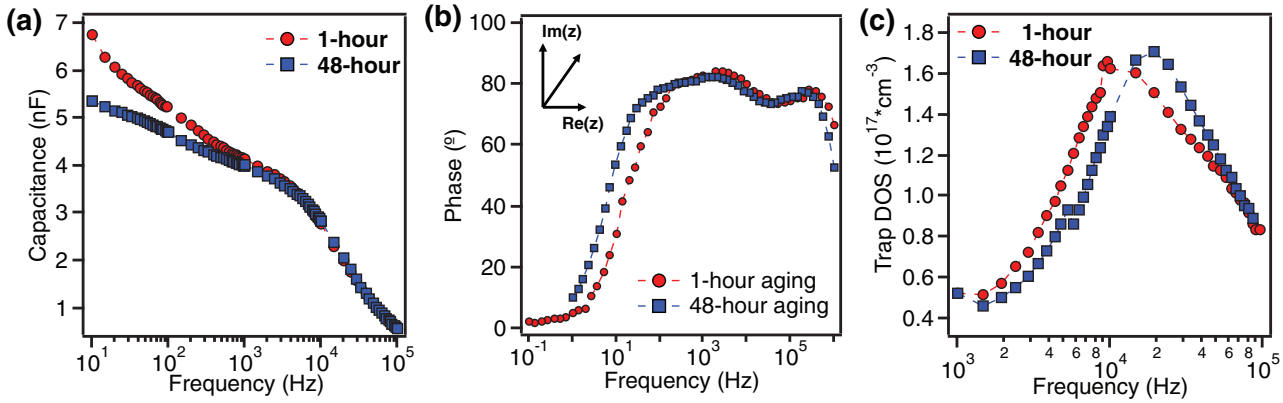

Figure 5. a) Capacitance as a function of AC field frequency for device produced by 1 h solution and 48 h solution for perovskite layer. b) Impedance phase angle analysis for both of those devices. c) Trap density of states calculated from panel (a) for both of devices.

film formation that can lead to high performance and reliable optoelectronic devices.

4. Experimental Section

Materials: Methylamine (33 wt% in absolute ethanol), hydrochloric acid (37 wt% in water), lead iodide (PbI_2, 99.99% purity), PCBM (>99.5%), and DMF (anhydrous, 98%) were purchased from Sigma-Aldrich and were used without further purification. PEDOT:PSS (PVP AI 4083) was purchased from Clevios. Patterned ITO substrates (150 nm, 7 $\Omega\ \square^{-1}$) were purchased from Thin Film Device Inc.

Synthesis of Methylamine Hydrochloride (MACl): Methylamine hydrochloride synthesis procedure is reported elsewhere.[3,49] Generally, dissolved 10 mL of methylamine and 50 mL of diethyl ether in 100 mL round-bottomed flask and then immersed in ice bath for 20 min, followed by the addition of 12 mL of hydrochloric acid (37 wt% in water) drop wise. The resulted white precipitate was collected and washed with diethyl ether three times and then dried in a vacuum oven at 60 °C overnight.

Perovskite Precursor Preparation and Device Fabrication: The precursor preparation was made using 100 mg PbI_2 and equal molar of MACl in 1 mL of anhydrous DMF with constant stirring at 70 °C for various time (from 1 to 48 h) for the thin-film samples and device fabrication. The AFM samples were prepared by taking the various aged solution and spun cast at room temperature with 5000 rpm for 40 s. The substrate preparation for device was performed following the procedure described in previous papers.[3,40,49] Generally, the perovskite precursor solutions were heated at 70 °C and then spun cast on a substrate preheated to 180 °C with 5000 rpm for 20 s. The PCBM solution (20 mg mL^{-1} in chlorobenzene) was spin coated at room temperature on top of the perovskite film at 1000 rpm for 45 s to form a 20 nm thick electron transport layer. Finally, the whole device was transferred to an inbuilt thermal evaporation chamber with pressure of 1e−7 Torr for thermal deposition of aluminum (Al) electrode. The Al top electrode was deposited through a mask that defined the device active area of 0.07 cm^2 for the solar cells.

Films Characterization: The thin film was obtained by our recently developed "hot-casting" method. Specifically, the substrates were preheated on a hotplate at 180 °C in an argon-filled glove box. Then, the substrates were immediately transferred onto a spin coater chunk. After dropping the precursors that were aged for various time, the solution was kept at 70 °C to prevent temperature quenching. The spin coat was started immediately, the spin rate was at 5000 rpm without ramp. After 5 s, the film turned dark brown color indicating that the perovskite phase was formed. The obtained thin films were taken for grazing incidence X-ray diffraction for structural characterization. GIXRD spectra from the perovskite films were obtained using an X-ray powder diffraction system (D5000, Siemens) with Cu Kα radiation ($l = 1.5406$ Å) at 0.05 per step with a holding time of 5 s per step under the operation conditions of 30 kV and 40 mA. Optical microscope images were collected using Olympus BX53M microscopy. Atomic force microscope images were collected from Bruker Multimode 8. The average domain size was calculated >50 grains from different optical images by using analyze function of Image J.

Device Characterization: The light current–voltage curves are taken under air mass 1.5 G 1 Sun solar simulator by applying voltage and collecting current using a Keithley 2400 unit. The light was simulated by a xenon-lamp-based solar simulator (Oriel LCS-100). A NIST calibrated monocrystalline silicon solar cell (Newport532, ISO1599) was used for light intensity calibration every time before measurement. All the solar cells were covered by a shadow mask to define the illumination area. The hysteresis curves were taken by scanning the voltage from forward bias to reverse bias (or from reverse bias to forward bias) with voltage settling time of 3 ms and voltage step of 0.02 V.

Supporting Information

Supporting Information is available from the Wiley Online Library or from the author.

Acknowledgements

This research was supported by the Laboratory Directed Research and Development (LDRD) program, under the auspices of Department of Energy (DOE).

Received: September 27, 2016
Revised: November 12, 2016
Published online: January 30, 2017

[1] NREL http://www.nrel.gov/ncpv/images/efficiency_chart.jpg, accessed: September 2016.
[2] M. A. Green, K. Emery, Y. Hishikawa, W. Warta, E. D. Dunlop, *Prog. Photovoltaics Res. Appl.* **2016**, *24*, 905.
[3] W. Nie, H. Tsai, R. Asadpour, J.-C. Blancon, A. J. Neukirch, G. Gupta, J. J. Crochet, M. Chhowalla, S. Tretiak, M. A. Alam, H.-L. Wang, A. D. Mohite, *Science* **2015**, *347*, 522.
[4] H. Tsai, W. Nie, J.-C. Blancon, C. C. Stoumpos, R. Asadpour, B. Harutyunyan, A. J. Neukirch, R. Verduzco, J. J. Crochet, S. Tretiak, L. Pedesseau, J. Even, M. A. Alam, G. Gupta, J. Lou, P. M. Ajayan, M. J. Bedzyk, M. G. Kanatzidis, A. D. Mohite, *Nature* **2016**, *536*, 312.
[5] X. Li, D. Bi, C. Yi, J.-D. Décoppet, J. Luo, S. M. Zakeeruddin, A. Hagfeldt, M. Grätzel, *Science* **2016**, DOI: 10.1126/science.aaf8060.
[6] M. Saliba, S. Orlandi, T. Matsui, S. Aghazada, M. Cavazzini, J.-P. Correa-Baena, P. Gao, R. Scopelliti, E. Mosconi, K.-H. Dahmen, F. De Angelis, A. Abate, A. Hagfeldt, G. Pozzi, M. Graetzel, M. K. Nazeeruddin, *Nat. Energy* **2016**, *1*, 15017.
[7] D. P. McMeekin, G. Sadoughi, W. Rehman, G. E. Eperon, M. Saliba, M. T. Hörantner, A. Haghighirad, N. Sakai, L. Korte, B. Rech, M. B. Johnston, L. M. Herz, H. J. Snaith, *Science* **2016**, *351*, 151.
[8] D. Shi, V. Adinolfi, R. Comin, M. Yuan, E. Alarousu, A. Buin, Y. Chen, S. Hoogland, A. Rothenberger, K. Katsiev, Y. Losovyj, X. Zhang, P. A. Dowben, O. F. Mohammed, E. H. Sargent, O. M. Bakr, *Science* **2015**, *347*, 519.
[9] X. Li, M. Ibrahim Dar, C. Yi, J. Luo, M. Tschumi, S. M. Zakeeruddin, M. K. Nazeeruddin, H. Han, M. Grätzel, *Nat. Chem.* **2015**, *7*, 703.
[10] D. W. de Quilettes, S. M. Vorpahl, S. D. Stranks, H. Nagaoka, G. E. Eperon, M. E. Ziffer, H. J. Snaith, D. S. Ginger, *Science* **2015**, *348*, 683.
[11] N. J. Jeon, J. H. Noh, Y. C. Kim, W. S. Yang, S. Ryu, S. Il Seok, *Nat. Mater.* **2014**, *13*, 897.
[12] J.-H. Im, I.-H. Jang, N. Pellet, M. Grätzel, N.-G. Park, *Nat. Nano* **2014**, *9*, 927.
[13] M. M. Lee, J. Teuscher, T. Miyasaka, T. N. Murakami, H. J. Snaith, *Science* **2012**, *338*, 643.
[14] L. Dou, A. B. Wong, Y. Yu, M. Lai, N. Kornienko, S. W. Eaton, A. Fu, C. G. Bischak, J. Ma, T. Ding, N. S. Ginsberg, L.-W. Wang, A. P. Alivisatos, P. Yang, *Science* **2015**, *349*, 1518.
[15] J. You, L. Meng, T.-B. Song, T.-F. Guo, Y. Yang, W.-H. Chang, Z. Hong, H. Chen, H. Zhou, Q. Chen, Y. Liu, N. De Marco, Y. Yang, *Nat. Nanotechnol.* **2016**, *11*, 75.
[16] W. S. Yang, J. H. Noh, N. J. Jeon, Y. C. Kim, S. Ryu, J. Seo, S. Il Seok, *Science* **2015**, *348*, 1234.
[17] M. A. Green, A. Ho-Baillie, H. J. Snaith, *Nat. Photonics* **2014**, *8*, 506.
[18] S. De Wolf, J. Holovsky, S.-J. Moon, P. Löper, B. Niesen, M. Ledinsky, F.-J. Haug, J.-H. Yum, C. Ballif, *J. Phys. Chem. Lett.* **2014**, *5*, 1035.
[19] C. Wehrenfennig, G. E. Eperon, M. B. Johnston, H. J. Snaith, L. M. Herz, *Adv. Mater.* **2014**, *26*, 1584.
[20] H. Oga, A. Saeki, Y. Ogomi, S. Hayase, S. Seki, *J. Am. Chem. Soc.* **2014**, *136*, 13818.

[21] G. Xing, N. Mathews, S. Sun, S. S. Lim, Y. M. Lam, M. Grätzel, S. Mhaisalkar, T. C. Sum, *Science* **2013**, *342*, 344.
[22] S. D. Stranks, G. E. Eperon, G. Grancini, C. Menelaou, M. J. P. Alcocer, T. Leijtens, L. M. Herz, A. Petrozza, H. J. Snaith, *Science* **2013**, *342*, 341.
[23] Z. Yuan, Y. Shu, Y. Xin, B. Ma, *Chem. Commun.* **2016**, *52*, 3887.
[24] K. Yao, X. Wang, Y. Xu, F. Li, L. Zhou, *Chem. Mater.* **2016**, *28*, 3131.
[25] M. C. Weidman, M. Seitz, S. D. Stranks, W. A. Tisdale, *ACS Nano* **2016**, *10*, 7830.
[26] C. C. Stoumpos, D. H. Cao, D. J. Clark, J. Young, J. M. Rondinelli, J. I. Jang, J. T. Hupp, M. G. Kanatzidis, *Chem. Mater.* **2016**, *28*, 2852.
[27] L. N. Quan, M. Yuan, R. Comin, O. Voznyy, E. M. Beauregard, S. Hoogland, A. Buin, A. R. Kirmani, K. Zhao, A. Amassian, D. H. Kim, E. H. Sargent, *J. Am. Chem. Soc.* **2016**, *138*, 2649.
[28] M. E. Kamminga, H.-H. Fang, M. R. Filip, F. Giustino, J. Baas, G. R. Blake, M. A. Loi, T. T. M. Palstra, *Chem. Mater.* **2016**, *28*, 4554.
[29] D. H. Cao, C. C. Stoumpos, O. K. Farha, J. T. Hupp, M. G. Kanatzidis, *J. Am. Chem. Soc.* **2015**, *137*, 7843.
[30] S. Zhang, P. Audebert, Y. Wei, J.-S. Lauret, L. Galmiche, E. Deleporte, *J. Mater. Chem.* **2011**, *21*, 466.
[31] L. Mao, H. Tsai, W. Nie, L. Ma, J. Im, C. C. Stoumpos, C. D. Malliakas, F. Hao, M. R. Wasielewski, A. D. Mohite, M. G. Kanatzidis, *Chem. Mater.* **2016**, *28*, 7781.
[32] L. Pedesseau, D. Sapori, B. Traore, R. Robles, H.-H. Fang, M. A. Loi, H. Tsai, W. Nie, J.-C. Blancon, A. Neukirch, S. Tretiak, A. D. Mohite, C. Katan, J. Even, M. Kepenekian, *ACS Nano* **2016**, *10*, 9776.
[33] Z. Xiao, W. Meng, B. Saparov, H.-S. Duan, C. Wang, C. Feng, W. Liao, W. Ke, D. Zhao, J. Wang, D. B. Mitzi, Y. Yan, *J. Phys. Chem. Lett.* **2016**, *7*, 1213.
[34] D. Umeyama, Y. Lin, H. I. Karunadasa, *Chem. Mater.* **2016**, *28*, 3241.
[35] B. Saparov, D. B. Mitzi, *Chem. Rev.* **2016**, *116*, 4558.
[36] G. Kieslich, S. Sun, A. K. Cheetham, *Chem. Sci.* **2014**, *5*, 4712.
[37] Y. Hu, J. Schlipf, M. Wussler, M. L. Petrus, W. Jaegermann, T. Bein, P. Müller-Buschbaum, P. Docampo, *ACS Nano* **2016**, *10*, 5999.
[38] I. C. Smith, E. T. Hoke, D. Solis-Ibarra, M. D. McGehee, H. I. Karunadasa, *Angew. Chem., Int. Ed.* **2014**, *53*, 11232.
[39] A. H. Slavney, R. W. Smaha, I. C. Smith, A. Jaffe, D. Umeyama, H. I. Karunadasa, *Inorg. Chem.* **2016**, DOI: 10.1021/acs.inorgchem.6b01336.
[40] W. Nie, J.-C. Blancon, A. J. Neukirch, K. Appavoo, H. Tsai, M. Chhowalla, M. A. Alam, M. Y. Sfeir, C. Katan, J. Even, S. Tretiak, J. J. Crochet, G. Gupta, A. D. Mohite, *Nat. Commun.* **2016**, *7*, 11574.
[41] J. Yang, B. D. Siempelkamp, D. Liu, T. L. Kelly, *ACS Nano* **2015**, *9*, 1955.
[42] E. T. Hoke, D. J. Slotcavage, E. R. Dohner, A. R. Bowring, H. I. Karunadasa, M. D. McGehee, *Chem. Sci.* **2015**, *6*, 613.
[43] S. Ito, S. Tanaka, K. Manabe, H. Nishino, *J. Phys. Chem. C* **2014**, *118*, 16995.
[44] J. H. Noh, S. H. Im, J. H. Heo, T. N. Mandal, S. Il Seok, *Nano Lett.* **2013**, *13*, 1764.
[45] T. Leijtens, G. E. Eperon, S. Pathak, A. Abate, M. M. Lee, H. J. Snaith, *Nat. Commun.* **2013**, *4*, 2885.
[46] J.-C. Blancon, W. Nie, A. J. Neukirch, G. Gupta, S. Tretiak, L. Cognet, A. D. Mohite, J. J. Crochet, *Adv. Funct. Mater.* **2016**, *26*, 4283.
[47] M. Liu, M. B. Johnston, H. J. Snaith, *Nature* **2013**, *501*, 395.
[48] C. M. M. Soe, C. C. Stoumpos, B. Harutyunyan, E. F. Manley, L. X. Chen, M. J. Bedzyk, T. J. Marks, M. G. Kanatzidis, *ChemSusChem* **2016**, *9*, 2656.
[49] H. Tsai, W. Nie, P. Cheruku, N. H. Mack, P. Xu, G. Gupta, A. D. Mohite, H.-L. Wang, *Chem. Mater.* **2015**, *27*, 5570.
[50] S. T. Williams, F. Zuo, C.-C. Chueh, C.-Y. Liao, P.-W. Liang, A. K. Y. Jen, *ACS Nano* **2014**, *8*, 10640.
[51] M. Saliba, K. W. Tan, H. Sai, D. T. Moore, T. Scott, W. Zhang, L. A. Estroff, U. Wiesner, H. J. Snaith, *J. Phys. Chem. C* **2014**, *118*, 17171.
[52] J. Kim, S.-H. Lee, J. H. Lee, K.-H. Hong, *J. Phys. Chem. Lett.* **2014**, *5*, 1312.
[53] S. Colella, E. Mosconi, P. Fedeli, A. Listorti, F. Gazza, F. Orlandi, P. Ferro, T. Besagni, A. Rizzo, G. Calestani, G. Gigli, F. De Angelis, R. Mosca, *Chem. Mater.* **2013**, *25*, 4613.
[54] W. Zhang, M. Saliba, D. T. Moore, S. K. Pathak, M. T. Hörantner, T. Stergiopoulos, S. D. Stranks, G. E. Eperon, J. A. Alexander-Webber, A. Abate, A. Sadhanala, S. Yao, Y. Chen, R. H. Friend, L. A. Estroff, U. Wiesner, H. J. Snaith, *Nat. Commun.* **2015**, *6*, 6142.
[55] G. E. Eperon, V. M. Burlakov, P. Docampo, A. Goriely, H. J. Snaith, *Adv. Funct. Mater.* **2014**, *24*, 151.
[56] A. Dualeh, N. Tétreault, T. Moehl, P. Gao, M. K. Nazeeruddin, M. Grätzel, *Adv. Funct. Mater.* **2014**, *24*, 3250.
[57] J. M. Azpiroz, E. Mosconi, J. Bisquert, F. De Angelis, *Energy Environ. Sci.* **2015**, *8*, 2118.
[58] W.-J. Yin, T. Shi, Y. Yan, *Appl. Phys. Lett.* **2014**, *104*, 63903.
[59] F. Zhang, W. Ma, H. Guo, Y. Zhao, X. Shan, K. Jin, H. Tian, Q. Zhao, D. Yu, X. Lu, G. Lu, S. Meng, *Chem. Mater.* **2016**, *28*, 802.
[60] S. Meloni, T. Moehl, W. Tress, M. Franckevičius, M. Saliba, Y. H. Lee, P. Gao, M. K. Nazeeruddin, S. M. Zakeeruddin, U. Rothlisberger, M. Graetzel, *Nat. Commun.* **2016**, *7*, 10334.
[61] C. Eames, J. M. Frost, P. R. F. Barnes, B. C. O'Regan, A. Walsh, M. S. Islam, *Nat. Commun.* **2015**, *6*, 7497.
[62] N. K. Noel, A. Abate, S. D. Stranks, E. S. Parrott, V. M. Burlakov, A. Goriely, H. J. Snaith, *ACS Nano* **2014**, *8*, 9815.
[63] H. Yu, H. Lu, F. Xie, S. Zhou, N. Zhao, *Adv. Funct. Mater.* **2016**, *26*, 1411.
[64] B.-E. Cohen, S. Aharon, A. Dymshits, L. Etgar, *J. Phys. Chem. C* **2016**, *120*, 142.
[65] Y. Zhao, K. Zhu, *J. Mater. Chem. A* **2015**, *3*, 9086.
[66] H.-S. Ko, J.-W. Lee, N.-G. Park, *J. Mater. Chem. A* **2015**, *3*, 8808.
[67] Z. Xiao, Q. Dong, C. Bi, Y. Shao, Y. Yuan, J. Huang, *Adv. Mater.* **2014**, *26*, 6503.
[68] J. Liu, C. Gao, X. He, Q. Ye, L. Ouyang, D. Zhuang, C. Liao, J. Mei, W. Lau, *ACS Appl. Mater. Interfaces* **2015**, *7*, 24008.
[69] P. Prajongtat, T. Dittrich, *J. Phys. Chem. C* **2015**, *119*, 9926.
[70] C.-H. Chiang, C.-G. Wu, *Nat. Photonics* **2016**, *10*, 196.
[71] Y. C. Zheng, S. Yang, X. Chen, Y. Chen, Y. Hou, H. G. Yang, *Chem. Mater.* **2015**, *27*, 5116.
[72] C. Bi, Q. Wang, Y. Shao, Y. Yuan, Z. Xiao, J. Huang, *Nat. Commun.* **2015**, *6*, 7747.
[73] N. T. K. Thanh, N. Maclean, S. Mahiddine, *Chem. Rev.* **2014**, *114*, 7610.
[74] R. Viswanatha, D. D. Sarma, in *Nanomaterials Chemistry*, Wiley-VCH, Weinheim, **2007**, pp. 139–170.
[75] V. K. LaMer, *Ind. Eng. Chem.* **1952**, *44*, 1270.
[76] V. K. LaMer, R. H. Dinegar, *J. Am. Chem. Soc.* **1950**, *72*, 4847.
[77] A. Binek, I. Grill, N. Huber, K. Peters, A. G. Hufnagel, M. Handloser, P. Docampo, A. Hartschuh, T. Bein, *Chem. - Asian J.* **2016**, *11*, 1199.
[78] Q. Chen, H. Zhou, Y. Fang, A. Z. Stieg, T.-B. Song, H.-H. Wang, X. Xu, Y. Liu, S. Lu, J. You, P. Sun, J. McKay, M. S. Goorsky, Y. Yang, *Nat. Commun.* **2015**, *6*, 7269.
[79] H. Yu, F. Wang, F. Xie, W. Li, J. Chen, N. Zhao, *Adv. Funct. Mater.* **2014**, *24*, 7102.

[80] K. G. Stamplecoskie, J. S. Manser, P. V Kamat, *Energy Environ. Sci.* **2015**, *8*, 208.
[81] A. Baldan, *J. Mater. Sci.* **2002**, *37*, 2171.
[82] M. Yang, T. Zhang, P. Schulz, Z. Li, G. Li, D. H. Kim, N. Guo, J. J. Berry, K. Zhu, Y. Zhao, *Nat. Commun.* **2016**, *7*, 12305.
[83] D. T. Moore, H. Sai, K. W. Tan, D.-M. Smilgies, W. Zhang, H. J. Snaith, U. Wiesner, L. A. Estroff, *J. Am. Chem. Soc.* **2015**, *137*, 2350.
[84] N. Kitazawa, Y. Watanabe, Y. Nakamura, *J. Mater. Sci.* **2002**, *37*, 3585.
[85] Y. Tidhar, E. Edri, H. Weissman, D. Zohar, G. Hodes, D. Cahen, B. Rybtchinski, S. Kirmayer, *J. Am. Chem. Soc.* **2014**, *136*, 13249.
[86] J. Kim, T. Hwang, S. Lee, B. Lee, J. Kim, G. S. Jang, S. Nam, B. Park, *Sci. Rep.* **2016**, *6*, 25648.
[87] I. M. Lifshitz, V. V. Slyozov, *J. Phys. Chem. Solids* **1961**, *19*, 35.
[88] D. P. Almond, C. R. Bowen, *J. Phys. Chem. Lett.* **2015**, *6*, 1736.